ELSEVIER

Polymer 40 (1999) 2699–2709

polymer

Nylon 6 as a modifier for maleated ethylene–propylene elastomers

O. Okada[1], H. Keskkula, D.R. Paul*

Department of Chemical Engineering, The University of Texas at Austin, Austin, TX 78712, USA
Center for Polymer Research, The University of Texas at Austin, Austin, TX 78712, USA

Received 6 February 1998; revised 8 June 1998; accepted 23 June 1998

Abstract

Blends of nylon 6 and ethylene–propylene rubber, grafted with maleic anhydride, (EPR-g-MA) were prepared using a melt blending process. For certain compositions, nylon 6 forms finely dispersed particles due to the reaction of the polyamide amine end groups with the grafted maleic anhydride, that have the potential to reinforce the elastomer matrix. This study focuses on the effects of the content of nylon 6 on the rheological, morphological and mechanical properties of such blends where nylon 6 is the dispersed phase. Transmission electron microscopy was used to determine blend morphology. Mechanical properties were examined by stress–strain measurements and dynamic mechanical thermal measurements; the modulus is compared to values calculated from theory. The addition of magnesium oxide causes significant improvement in tensile properties of these blends.

Keywords: Maleated EPR; Nylon 6; Blends

1. Introduction

A wide range of polymeric materials with elastomeric properties that can be fabricated by melt processing procedures used for thermoplastics, known as thermoplastic elastomers (TPE), have achieved significant commercial importance over the last 20 years or more [1]. One approach to formation of such materials is block copolymerization, where soft and hard segments are appropriately arranged to obtain desirable mechanical behavior; important examples of this type include triblock structures containing styrene/diene [2,3] segments formed by anionic polymerization and segmented copolymers based on polyester [4–6] or polyurethane [7–13] condensation polymerizations. Another approach involves melt blending of elastomeric materials with rigid thermoplastics [5,6,8,13–18]. Thermoplastic elastomers, whether based on block copolymers or blends, must contain two polymeric phases that have widely different softening temperatures so that at use temperatures, one phase is rubbery and the other is either glassy or crystalline [3,9,10,14–16,19,20].

In a melt blending approach, it is feasible to use chemical reactivity of the component polymers to achieve TPE materials with controlled morphology and chemical bonding between the matrix and the dispersed phases. Rubber toughening of polyamides with maleated elastomers may serve as a model for this approach [21–23]. In such blends, reaction of the polyamide amine end groups with the grafted maleic anhydride leads to polyamide-rubber graft copolymer via imide linkages which enable the formation of rubber particles of about 0.1 to 0.5 μm in diameter dispersed in the polyamide matrix [24–29]. Control of morphology (particle size or interparticle distance) is key to super tough, rigid materials. By varying the ratio of maleated rubber to polyamide, it should be possible to make fine polyamide particles dispersed in a rubbery matrix. When stressed, the rigid particles should provide some degree of resistance to flow or creep of the elastomer matrix (or physical crosslinking) due to the chemical bonding of these particles to the matrix; such mixtures should approximate TPE behavior since above the polyamide melting point melt processing should also be possible. Within the limits of phase inversion it should be possible to control the stiffness or hardness of such blends by the elastomer/polyamide ratio.

The morphology and structure–property relationships for thermoplastic elastomers prepared by this approach have been reported by Thamm et al. [30], based on graft copolymers of polypivalolactone and ethylene/propylene/diene monomer, EPDM, terpolymers. Burlett et al. [31–33] have also reported on elastomer-based alloys with thermoplastic

* Corresponding author.
[1] Permanent address: Bridgestone Corporation, 1, Kashio-cho, Totsuka-ku, Yokohama 244, Japan.

0032-3861/99/$ - see front matter
PII: S0032-3861(98)00497-2

Table 1
Materials used in this work

Polymer	Commerical designation	Characterization[a]	Molecular weight[a]	Brabender torque[b] (N·m)	Source
Nylon 6	Capron 8207F	End-group content: $[NH_2] = 47.9\ \mu eq\ g^{-1}$ $[COOH] = 43.0\ \mu eq\ g^{-1}$	$\bar{M}_n = 22,000$	5.4	AlliedSignal Inc.
Nylon 6	Ultramid B0	End-group content: $[NH_2] = 74.2\ \mu eq\ g^{-1}$ $[COOH] = 77.0\ \mu eq\ g^{-1}$	$\bar{M}_n = 13,200$	2.0	BASF Corp.
EPR-g-MA	Exxelor 1803	43 wt% ethylene 53 wt% propylene 1.14 wt% MA	–	8.2	Exxon Chemical Co.

[a] Ref. [27].
[b] Torque value taken after 10 min at 240°C and 60 rpm.

polymers formed via reactive processing. This paper explores the use of the amine–anhydride reaction to produce TPE materials by melt blending nylon 6 with ethylene–propylene rubber grafted with maleic anhydride, EPR-g-MA. The morphology and the mechanical properties of such blends where nylon 6 is the dispersed phase are described here.

2. Experimental

Table 1 describes materials used in this study. The rubber type is a commercially available random ethylene/propylene copolymer grafted with maleic anhydride (EPR-g-MA) from Exxon Chemicals designated as Exxelor 1803. This rubber was blended with a nylon 6, Capron 8207 from AlliedSignal, with a medium molecular weight ($\bar{M}_n = 22\,000$) having balanced acid and amine end groups. A low molecular weight nylon 6 ($\bar{M}_n = 13\,200$) with equal acid and amine end groups, Ultramid B0, an experimental material from BASF, was hydrolyzed by two extrusion passes through the single screw extruder at 300°C and 10 rpm without prior drying to reduce its molecular weight and to increase its reactivity. An antioxidant, Irganox 1076, at the level of 0.2 wt% in the EPR-g-MA rubber was used in the blends.

Rheological properties were measured using a Brabender Plasticorder with a 50 cm^3 mixing head and standard rotors operated at 240°C and 60 rpm. Torque was recorded continuously as a function of mixing time.

The materials were dried before melt blending in a vacuum oven for a minimum of 16 h at 60°C for EPR-g-MA and at 80°C for nylon 6. Blends were prepared by vigorously mixing all components together and extruding twice at 240°C and 40 rpm in a Killion single screw extruder ($L/D = 30$, $D = 2.54$ cm) outfitted with an intensive mixing head. The blends were injection molded into tensile bars (ASTM D638 Type I) by an Arburg Allrounder injection molding machine.

Shore A hardness was measured with a Pacific Transducer durometer according to ASTM D2240. Stress–strain properties were measured at room temperature by an Instron Testing Machine according to ASTM D412 (1980) using a cross-head speed of from 5.08 to 50.8 cm/min. The permanent set after break was determined at 10 min after failure of tensile specimens. The hysteresis ratio was calculated from the area between the loading and unloading curve at a cross-head speed of 12.7 cm/min. The Young's modulus was measured from the initial slope of the stress–strain curve at a cross-head speed of 5.08 cm/min.

The dynamic mechanical properties were determined by a Polymer Laboratories DMTA at a frequency of 30 Hz. The temperature range of those measurements was from −100 to 100°C at a heating rate of 3°C/min.

The morphology of the blends was observed by a JEOL 200 CX transmission electron microscope (TEM) using ultra-thin sections (10 to 20 nm) cryogenically microtomed at −50°C perpendicular to the flow direction of injection molded bars. The nylon 6 phase was stained by exposure of the thin sections to a 2% aqueous solution of phosphotungstic acid,

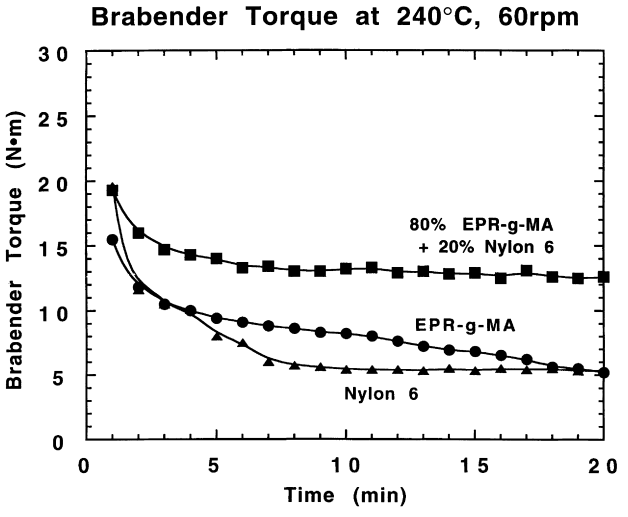

Fig. 1. Brabender torque response at 240°C and 60 rpm for nylon 6, EPR-g-MA and 80% EPR-g-MA/20% nylon 6 blend.

Table 2
The physical properties and particle size of EPR-g-MA/nylon 6 blends

Nylon 6 (%)	Hardness (Shore A)	Modulus at 50% elongation (MPa)	Tensile strength MPa	Elongation at break (%)	Set after break (%)	T_g (°C)	$\overline{d_w}$ (μm)	$\overline{d_w}/\overline{d_n}$
0	48	0.27	0.28	380	42.3	−38.5	–	–
5	49	0.33	0.36	260	24.3	−36.4	0.14	1.27
10	50	0.37	0.41	260	21.2	−35.7	0.17	1.28
15	53	0.47	0.53	220	19.8	−35.3	0.19	1.30
20	55	0.57	0.69	200	18.5	−35.1	0.23	1.43
30	68	1.07	1.20	130	7.2	−35.1	0.23	1.42
40	83	N/A	6.23	30	4.5	−34.3	0.30	1.50

PTA, for 30 min at room temperature. The TEM was operated at an accelerating voltage of 120 kV. Nylon 6 particle size was determined by a semi-automatic digital analysis technique using IMAGE® software from the National Institutes of Health.

3. Morphology

The grafting of nylon 6 to EPR-g-MA causes changes in rheological behavior which can be monitored during melt blending in a Brabender mixer. Fig. 1 shows that while nylon 6 and EPR-g-MA have relatively similar melt viscosities at 240°C, the 80/20 blend of EPR-g-MA/nylon 6 develops a torque of more than twice that of the individual blend components. It is apparent that the reaction between the two components is very rapid, since the high torque of the blend is established early in the experiment while the charge to the Brabender begins to be heated and fluxed.

The graft copolymer formed in situ by the reaction of the nylon 6 amine end groups with maleic anhydride in EPR-g-MA acts as a compatibilizer that leads to a very fine dispersion of the nylon 6 phase in the rubber matrix largely by limiting the frequency of particle–particle coalescence. In addition, the presence of the rubber/polyamide graft copolymer at the domain interfaces results in chemical bonding of the nylon 6 particles to the rubber matrix. The result should be a material with stable morphology and good adhesion between the hard and soft phases [34–36].

Fig. 2 shows the morphology of blends containing 5 to 50% nylon 6 in EPR-g-MA. The samples for microscopy were taken from the center of injection molded test bars across the flow direction. The nylon 6 particle size and size distribution are shown in Table 2 and Fig. 3. Some increase in particle size is noted as the nylon 6 content is increased from 5 to 30%. At 40% nylon 6, the polyamide particles are elongated with evidence of co-continuity of the phases; at 50% nylon 6 this is more obvious. At 60% nylon 6, the phase inversion is complete and EPR-g-MA is now the dispersed phase within the nylon 6 matrix.

4. Mechanical properties

The Shore A hardness of these blends increases steadily with nylon 6 content, as seen in Fig. 4. The increase is rather modest up to 16.5 vol% (20 wt%) of nylon 6 and then becomes more dramatic.

Typical stress–strain curves for the blends are shown in Fig. 5; selected properties are summarized in Table 2. These results were obtained at a cross-head speed of 12.7 cm/min; results for other testing speeds from 5 to 51 cm/min are shown in Fig. 6 for a blend containing 20% nylon 6. These data indicate an increase in the peak stress of about 30% and a shift in the stress peak to a slightly lower extension (from about 120 to 100%) as the rate of extension is increased from 5 to 51 cm/min. The two highest extension rates give rise to the highest failure elongations. Fig. 7

Table 3
Physical properties and particule size of EPR-g-MA/nylon 6 blends

Composition	Hardness (Shore A)	Modulus at 50% elongation (MPa)	Maximum strength (MPa)	Elongation at break (%)	Set after break (%)	Hysteresis loss (%)	$\overline{d_w}$ (μm)	T_g (°C)
100% EPR-g-MA	48	0.27	0.28	380	42.3	66.4	–	−38.5
80% EPR-g-MA + 20% nylon 6	55	0.57	0.69	200	18.5	65.4	0.23	−35.1
80% EPR-g-MA + 20% hydrolyzed nylon 6	55	0.63	0.84	190	17.9	66.0	0.15	−35.8
78.8% EPR-g-MA + 20% nylon 6 + 1.2% MgO	60	1.40	1.79	140	6.5	64.5	0.12	−34.5

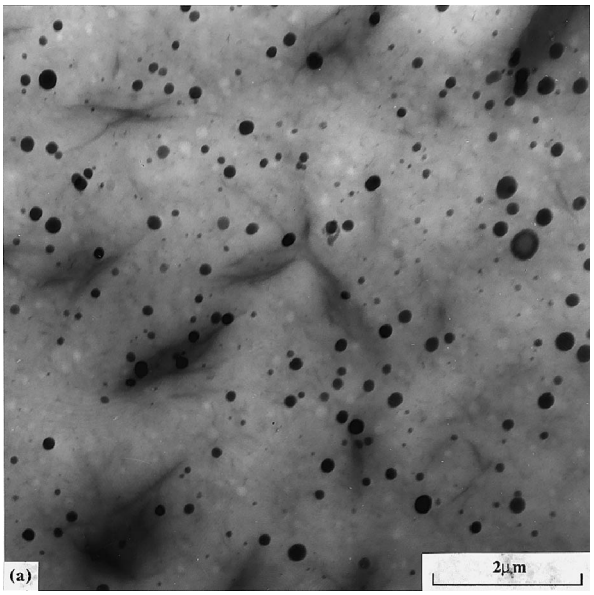
(a)
2μm

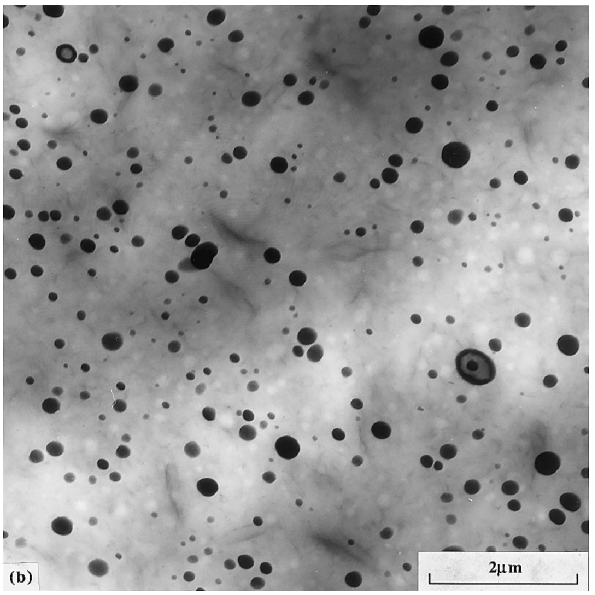
(b)
2μm

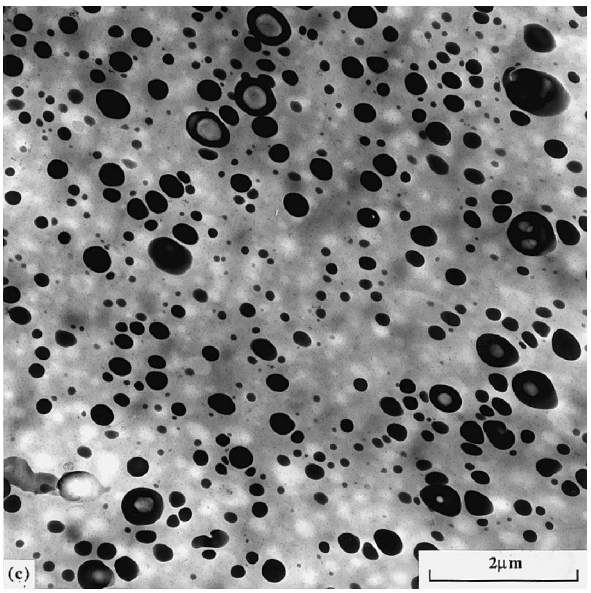
(c)
2μm

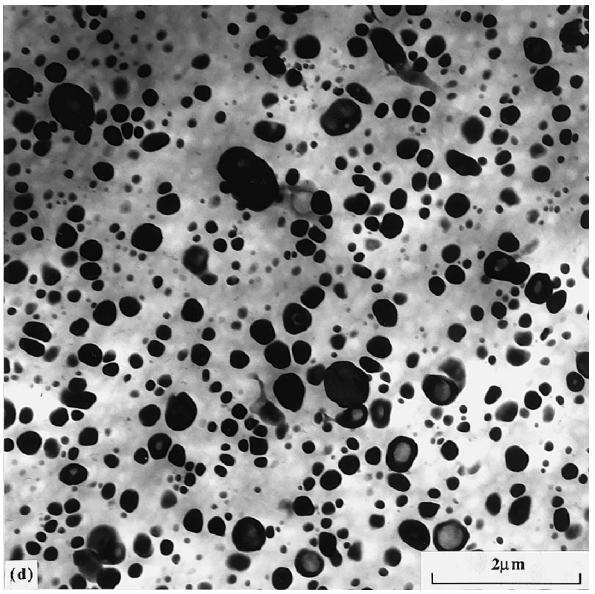
(d)
2μm

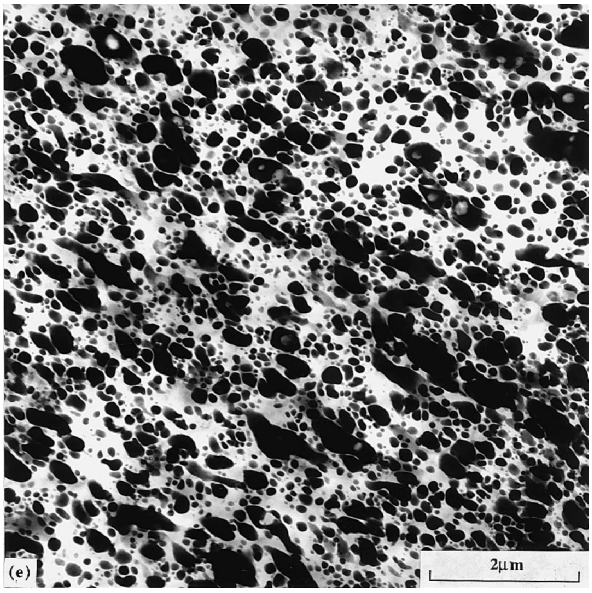
(e)
2μm

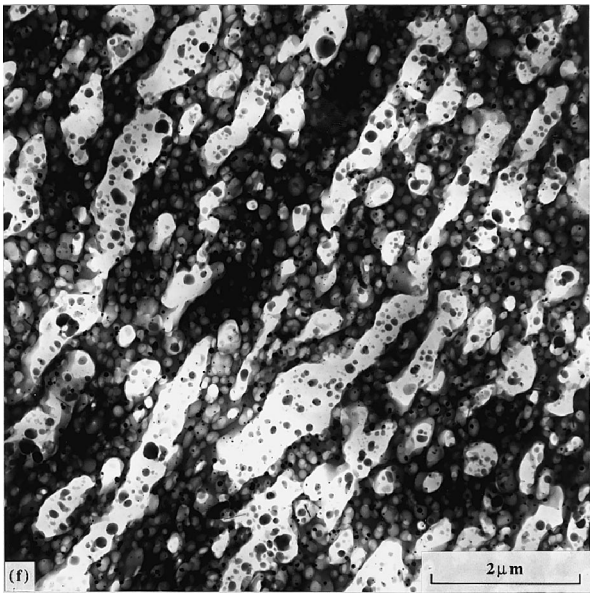
(f)
2μm

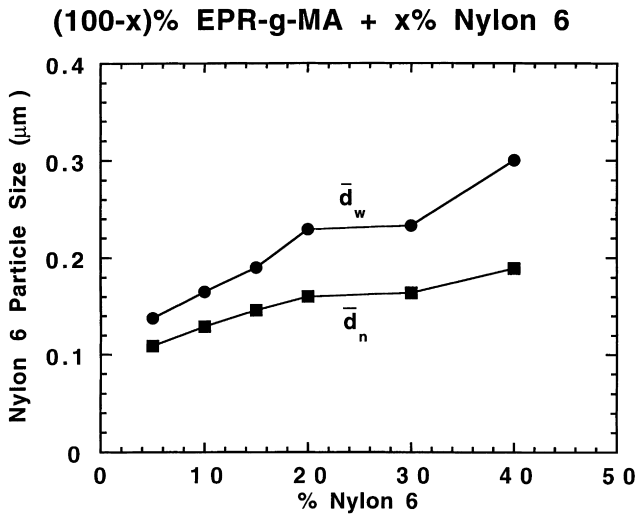

Fig. 3. Effect of nylon 6 content on weight and number average nylon 6 particle diameter for blends of (100 − *x*)% EPR-g-MA and *x*% nylon 6.

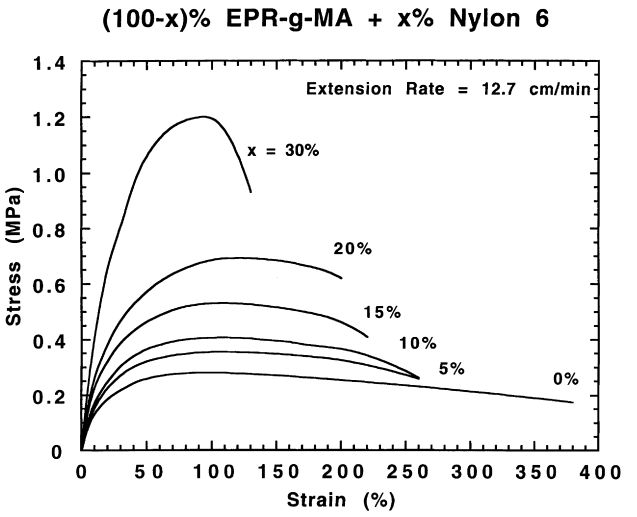

Fig. 5. Stress–strain properties for blends of (100 − *x*)% EPR-g-MA and *x*% nylon 6.

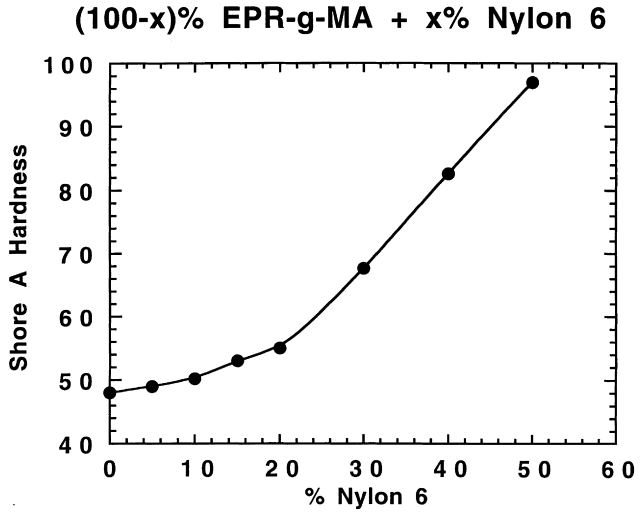

Fig. 4. Effect of nylon 6 content on Shore A hardness for blends of (100 − *x*)% EPR-g-MA and *x*% nylon 6.

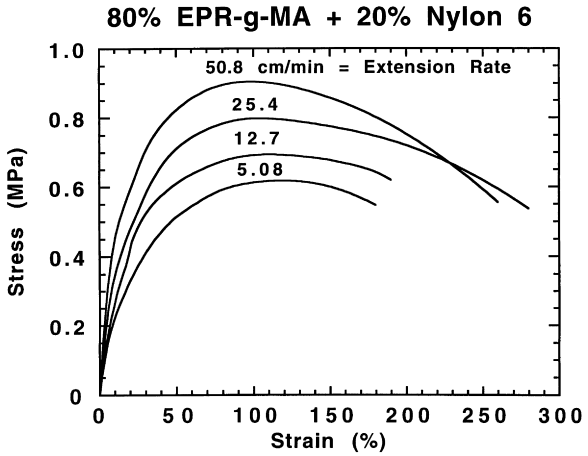

Fig. 6. Stress–strain diagrams for blends of 80% EPR-g-MA and 20% nylon 6 at various extension rates.

shows that for all blends the modulus increases noticeably as the testing speed increases.

The hysteresis loss, *H*, is given by

$$H = (W - W_r)/W$$

where *W* is the area under the first loading curve up to a particular strain (100%) and W_r is the corresponding area under the unloading curve [37]. The hysteresis behavior for a maximum strain of 100% strain is shown in Fig. 8 for an 80/20 EPR-g-MA/nylon 6 blend. The calculated hysteresis losses for this and other blends are given in Table 3. A hysteresis loss of 66% was determined for EPR-g-MA without any nylon 6 additive; incorporation of 20% nylon 6 does not significantly alter this measure of the mechanical loss process under the conditions used in this work.

Permanent set after break was found to be more or less independent of testing speed. As seen in Table 2, the addition of even small amounts of nylon 6 reduces the permanent set; it is substantially constant at about 20% for compositions containing 5–20% nylon 6 but drops to quite low levels for blends containing 30–40% nylon 6.

Fig. 9 shows typical stress–strain curves for three commercial TPE materials; a styrene–butadiene–styrene triblock, SBS (Kraton D1101), a styrene-hydrogenated butadiene–styrene triblock, SEBS (Kraton G1652) and a

Fig. 2. TEM photomicrographs of blends of *x*% nylon 6 and (100 − *x*)% EPR-g-MA: (a) $x = 5$, (b) $x = 10$, (c) $x = 20$, (d) $x = 30$, (e) $x = 40$, and (f) $x = 50$%.

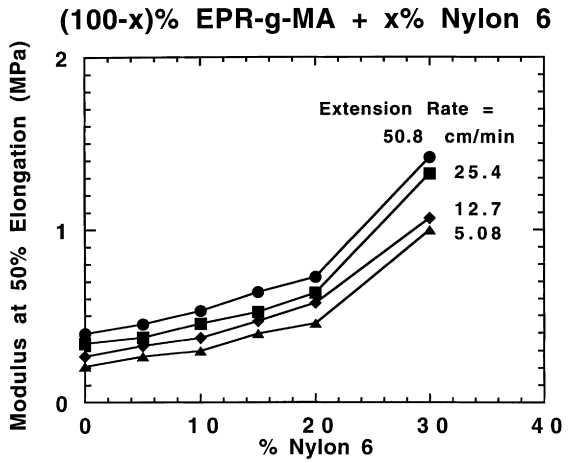

Fig. 7. Effect of nylon 6 content on the secant modulus (50% elongation) at various extension rates for blends of (100 − *x*)% EPR-g-MA and *x*% nylon 6.

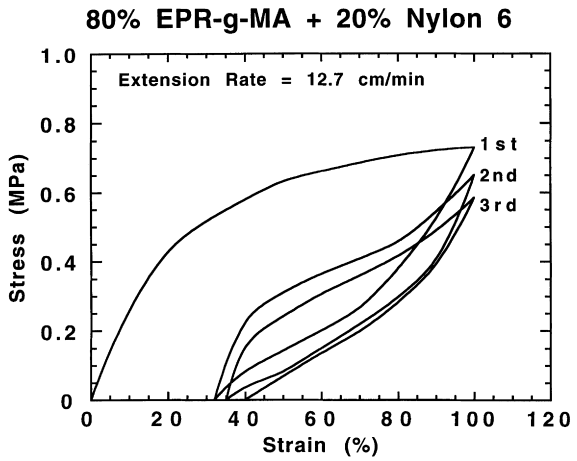

Fig. 8. Cyclic stress–strain behavior for blends of 80% EPR-g-MA and 20% nylon 6.

dynamically vulcanized polypropylene/ethylene–propylene rubber blend, Santoprene, having Shore A hardness values of 79, 71 and 55, respectively. Kraton G1652 shows a yield point at 10% elongation and a drawing process from 20 to 200% elongation. From 200% elongation to fracture, significant work hardening is observed [20,38]. The other materials showed no yield point, but a steady increase in stress before fracture. Both SBS and SEBS materials exhibit higher tensile strength than the Santoprene material. As seen from Table 2, these commercial TPE materials have higher Shore A hardness values than the typical 20% Nylon 6 and 80% EPR-g-MA blends examined in this study.

As seen from the comparison of stress–strain properties of the commercial TPE materials with the various blends of EPR-g-MA and nylon 6 (see Figs. 5 and 9), the latter have lower strength and exhibit stress softening which was not seen for any of the commercial TPE materials. Compared to the hard phases in triblock copolymer or dynamically vulcanized TPE materials, the nylon 6 phase is much less effective for reinforcing (stiffen or strengthen) the EPR-g-MA matrix or providing effective crosslinking to retard its viscoelastic relaxation during stress–strain testing.

Such behavior should be improved by having a greater number of chemical attachments between EPR-g-MA and nylon 6, and this can be achieved, in principle, by using a lower molecular weight of nylon 6 [39]. Calculations show that two nylon 6 grafts per EPR-g-MA molecule would be theoretically possible when the $\bar{M}_n$ of nylon 6 is less that 7000. There is no convenient source of such low molecular weight nylon 6 materials, so another approach was attempted. Ultramide BO is a very low molecular weight nylon 6 but its $\bar{M}_n$ is about twice the target value; one hydrolysis reaction per chain of this polymer should produce the desired level of amine functionality. In an attempt to obtain such a low $\bar{M}_n$ nylon 6, Ultramide B0 containing approximately 4.2% water was extruded twice at 300°C through a single screw extruder to effect hydrolysis [39–44]. As seen in Table 4, this procedure does lead to reduction of the nylon 6 molecular weight but not fully to the target value. Blends of this very low molecular weight nylon 6, produced by hydrolysis, with EPR-g-MA were prepared. These blends have a significantly reduced dispersed phase particle size (0.15 versus 0.23 μm for blends based on Capron 8207F); see Fig. 10. As seen in Fig. 11, blends based on the hydrolyzed nylon 6 do have somewhat improved tensile properties; however, their properties are still far below those of the other TPE materials whose stress–strain characteristics are shown in Fig. 9.

The addition of magnesium oxide to these blends was examined as another means to improve their mechanical

Table 4
Conditions for nylon 6 hydrolysis in a single screw extruder and resulting Brabender torque data

Material	Conditions of raw nylon 6 before extrusion		Extrusion temperature (°C)	Extruder (rpm)	Torque after 10 min (N·m)	$\overline{M_n^a}$
	Form of nylon	Drying				
Capron 8207F[a]	Granules	Yes	–	–	5.4	22 000
Ultramid BO[a]	Granules	Yes	–	–	2.0	13 200
Ultramid B0[b]	Powder	No	300	10	1.3	11 000[c]

[a] Pellets dried before Brabender experiment.
[b] Water content = 4.2 wt%.
[c] Molecular weight value estimated from Brabender torque/molecular weight relationship [27].

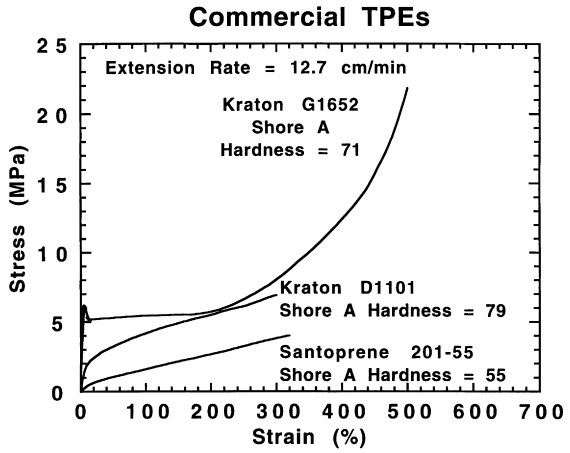

Fig. 9. Stress–strain properties for three commercial TPE materials.

performance. It has been reported that the addition of a small amount of MgO is effective for crosslinking of methacrylic acid containing elastomers [45,46]. Because of the carboxylic acid end-groups in nylon 6 and possibly some free acid groups in EPR-g-MA, this approach was considered to be potentially useful for improving the tensile properties of these blends.

Fig. 10(b) shows the effect of 1.2% MgO on the 80/20 EPR-g-MA/nylon 6 blend. Addition of MgO clearly contributes to reducing the particle size of nylon 6 domains (see Table 3) as found with the use of the hydrolyzed nylon 6. In Fig. 10(c), non-stained TEM photomicrographs show very small particles of MgO in this blend.

Fig. 12 shows that addition of MgO increases the melt viscosity of these blends as indicated by Brabender torque rheometry. A maximum effect is achieved at a loading level of 2% which gives rise to almost a two-fold increase in torque at 10 min. Torque rheometer data in Fig. 13 indicate that the addition of MgO to the other components of these blends shows no significant effect. Fig. 13(a) shows that the addition of MgO to the unmaleated EPR and its blend with nylon 6 has no effect on the torque response. Also, the effect of MgO on the blends with both of the elastomer components, i.e. EPR and EPR-g-MA is negligible (Fig. 13(b)). The lack of torque increases when MgO is added to EPR-g-MA is rather surprising in light of the data shown in Fig. 12. It implies the presence of some chemical synergism when the three principal blend components are melt blended together. No further explanation for this effect can be given at this time. As seen in Fig. 13(c), there is no effect on the torque response when MgO is melt blended with nylon 6. The fact that a torque increase is not seen on the addition of MgO to either EPR-g-MA or nylon 6 may be due

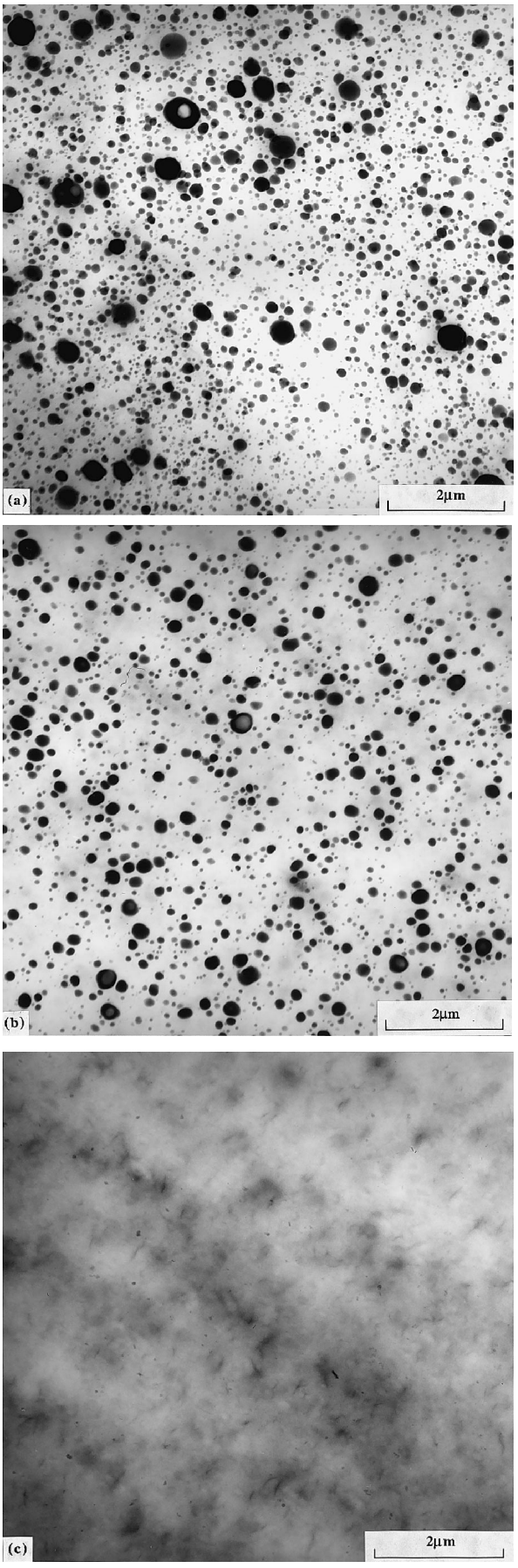

Fig. 10. TEM photomicrographs for: (a) blends of 80% EPR-g-MA and 20% hydrolyzed nylon 6; (b) blend of 78.8% EPR-g-MA and 20% nylon 6 containing 1.2% MgO, stained with phosphotungstic acid and (c) without staining.

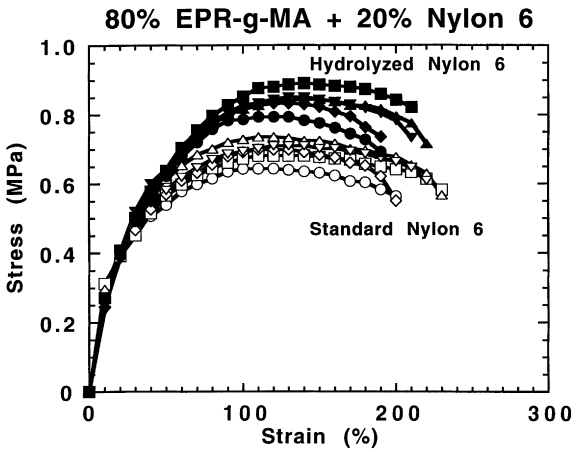

Fig. 11. Stress–strain curves for various individual samples of 80% EPR-g-MA and 20% nylon 6 blends showing difference between standard (open symbols) and hydrolyzed (solid symbols) nylon 6.

to the relative absence of water in these experiments or some presence of trace amount of moisture in the ternary blends that do show a torque increase.

The addition of small amounts of magnesium oxide to the blends causes significant improvement in tensile properties, as seen in Fig. 14. The maximum stress at 100% strain for the blend with 1.2% by weight of MgO is more than twice that of the corresponding blend without MgO. However, the strength is still significantly less than that of the Kraton and Santoprene materials, and there is no work hardening before ultimate fracture. It is suggested that the smaller nylon 6 particle size in these blends is caused by the increase of melt viscosity resulting from the presence of MgO which may lead to more grafting of nylon 6 to the EPR-g-MA. Together, these effects give rise to the improvement of the tensile properties of the blends of EPR-g-MA and nylon 6.

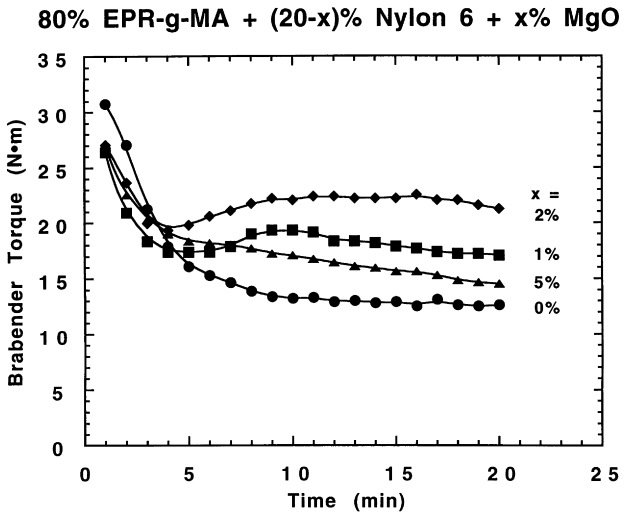

Fig. 12. Brabender torque response for blends of 80% EPR-g-MA and (20 − *x*)% nylon 6 containing *x*% MgO.

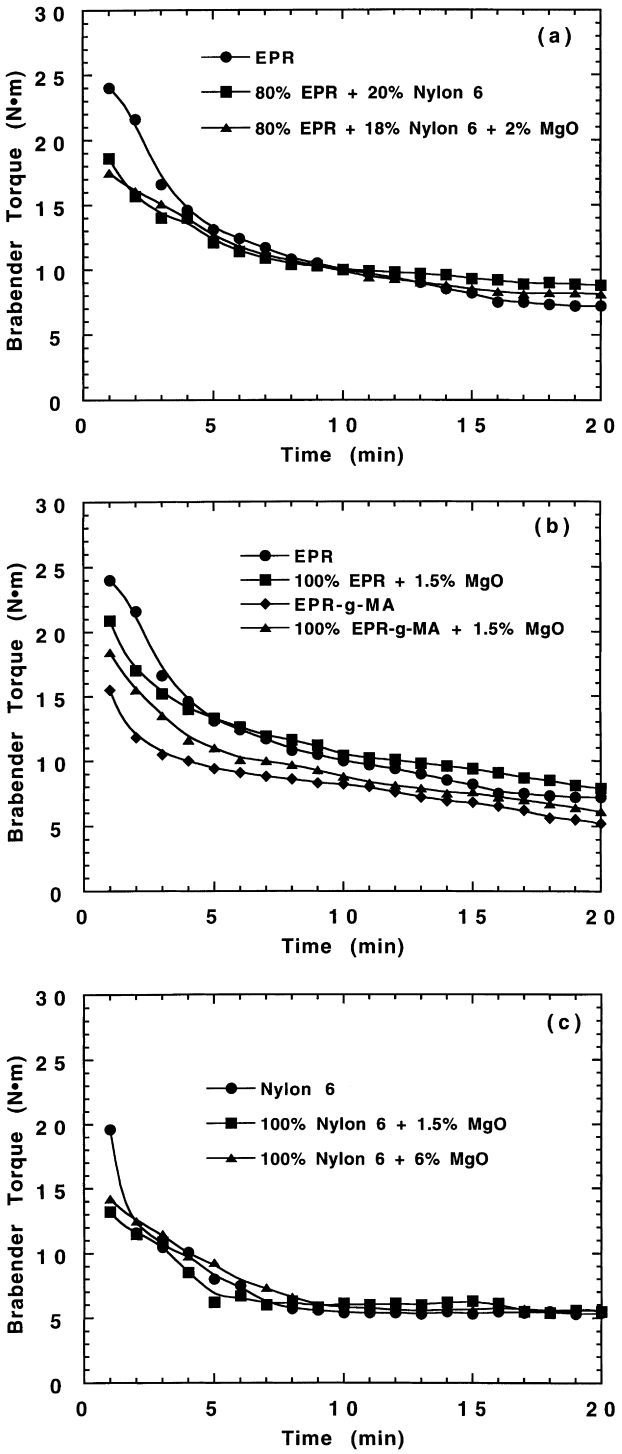

Fig. 13. Brabender torque response for: (a) blends of non-maleated EPR and nylon 6 with and without MgO; (b) mixtures of non-maleated EPR with MgO and EPR-g-MA with MgO; and (c) mixtures of nylon 6 and MgO.

The hysteresis loss at a strain of 100% for the 78.8/20/1.2 EPR-g-MA/nylon 6/MgO blends is shown in Fig. 15 and Table 3. In spite of the increased stress caused by MgO, the hysteresis loss is substantially the same at about 65% for both compositions.

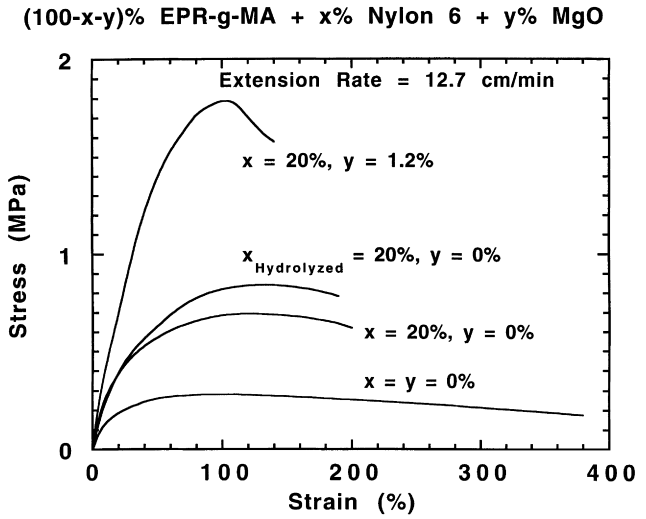

Fig. 14. Stress–strain properties for blends of (100 − *x* − *y*)% EPR-g-MA/*x*% nylon 6/*y*% MgO.

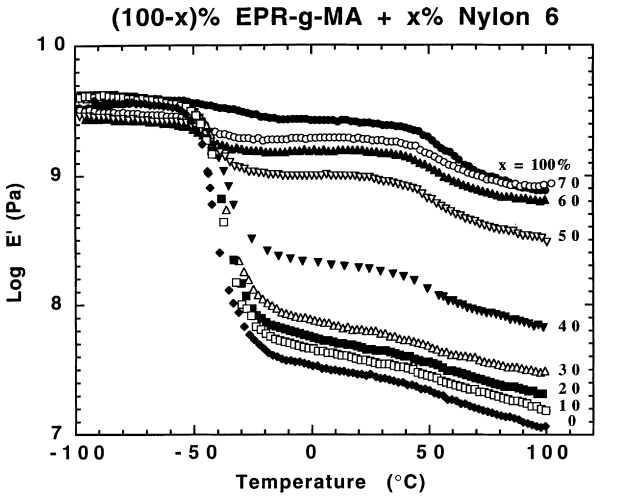

Fig. 16. Dynamic storage modulus for blends of (100 − *x*)% EPR-g-MA and *x*% nylon 6.

5. Dynamic mechanical properties

Blends of EPR-g-MA with nylon 6 over the entire composition range were characterized by measuring the dynamic mechanical properties at 30 Hz. The storage modulus, E', is shown as a function of temperature in Fig. 16; results for blends based on the hydrolyzed nylon 6 and those containing MgO are substantially the same as for the standard EPR-g-MA/nylon 6 blends. Loss tangent, tan δ, data are shown in Fig. 17. Two interesting trends deserve mention. First, as the nylon 6 content in the EPR-g-MA matrix increases from 0 to 40%, there is a decrease in magnitude of the rubber tan δ peak and a small increase in the temperature where this peak occurs (see T_g column in Table 2); over this range the dispersed nylon 6 phase particle size increases from 0.14 to 0.30 μm. Second, for compositions in the regions of phase inversion but where the rubber is the dispersed phase, the rubber phase tan δ peak is more typical of that for rubber toughened polymers such as ABS [47–50]. In styrene/acrylonitrile grafted polybutadiene rubbers the T_g of the grafted rubber is lower than that of the ungrafted rubber. In the current blends, the rubber phase T_g drops from −38 at 50% EPR-g-MA to −42°C at 30% EPR-g-MA. The rubber phase T_g peaks for the blends based on the hydrolyzed nylon 6 and the blends containing MgO are almost the same as those for the blends shown.

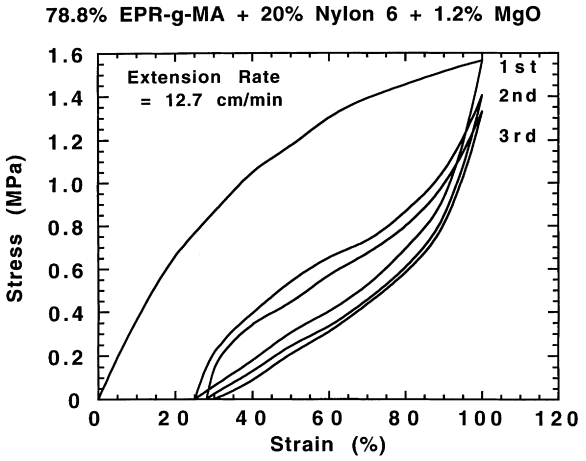

Fig. 15. Cyclic stress–strain behavior of blends of 78.8% EPR-g-MA, 20% nylon 6 and 1.2% MgO.

6. Modeling of modulus data

Experimental values of the tensile modulus, E, from stress–strain testing at 5.08 cm/min (Fig. 18(a)) and the storage modulus, E', from dynamic mechanical measurements (Fig. 18(b)) are shown for blends encompassing the whole composition range. These data represent compositions where there are nylon 6 particles in the EPR-g-MA matrix, continuing through the phase inversion to compositions where the EPR-g-MA particles are dispersed in the nylon 6 matrix. Equations for composite materials by Kerner [51], Faucher [52], and Hill [53] were considered for modeling these experimental results. Additional approaches for predicting elastic moduli for blends of hard and soft polymers phases have been reported [54]. The self-consistent theory proposed by Hill appears to give the best representation of the current experimental data and is probably the most sound from a mathematical point of view [55]. This model has the form

$$\left[\frac{\phi_1 K_1}{K_1+\frac{4}{3}G}+\frac{\phi_2 K_2}{K_2\frac{4}{3}G}\right]+5\left[\frac{\phi_1 G_2}{G-G_2}+\frac{\phi_2 G_1}{G-G_1}\right]+2=0 \quad (1)$$

where K is the bulk modulus and G is the shear modulus of the blend, while the corresponding component elastic

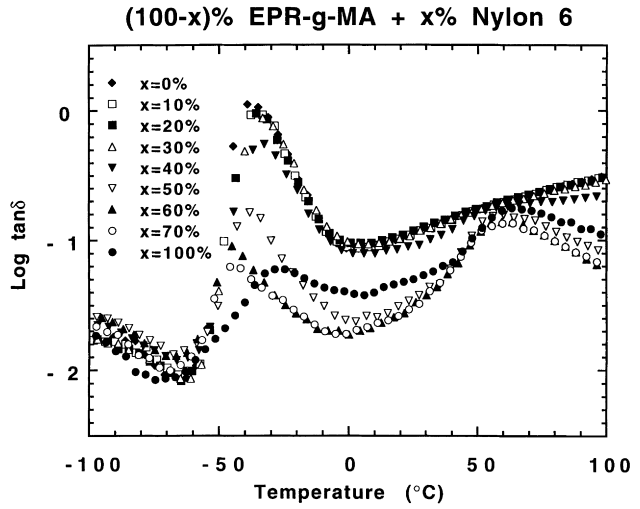

Fig. 17. Tan δ curves for blends of $(100-x)$% EPR-g-MA and x% nylon 6.

properties of each component have the appropriate subscript and ϕ_i is the volume fraction of component i.

Standard relations of elastic theory are used to relate the tensile modulus, E_i, to the bulk, K_i, and shear, G_i, moduli of each component (or the blend) via the Poisson ratio, ν_i,

$$K_i = \frac{E_i}{3(1-2\nu_1)} \text{ and } G_i = \frac{E_i}{2(1+\nu_i)} \quad (2)$$

Poisson's ratio was assumed to be 0.49 for EPR-g-MA and 0.33 for nylon 6 [56] and to be a linear function of composition for the blends. The solid lines shown in Fig. 18(a) and (b) were calculated using Hill's theory. As it turns out, the calculated results for the blends are quite insensitive to the assumption about the composition dependence of Poisson's ratio. Quite similar results were calculated by assuming $\nu = 0.49$ for all blends where the rubber is in the continuous phase and $\nu = 0.33$ for all blends where nylon 6 is the continuous phase. The values for the dynamic storage modulus E' are essentially the same as those for tensile modulus E measured in stress–strain tests when nylon 6 forms the matrix. However, the values of E are noticeably smaller than the corresponding E' values [57] in blends where the rubber phase is the matrix. It is interesting to note that the experimental points from the dynamic measurements agree better with the calculated curve up to about 35 vol% of nylon 6 than those of the stress–strain measurements. This range corresponds to blends where nylon 6 is dispersed as discrete particles in EPR-g-MA. Beyond phase inversion, where rubber particles are dispersed in the nylon 6 matrix, a larger deviation from the calculated values is apparent in both measurements. The largest deviation in both cases occurs for compositions in the phase inversion region. As this model does not consider the phase inversion issue, there is no appropriate way to deal with the deviations of calculated modulus values from the experimental ones in the phase inversion region.

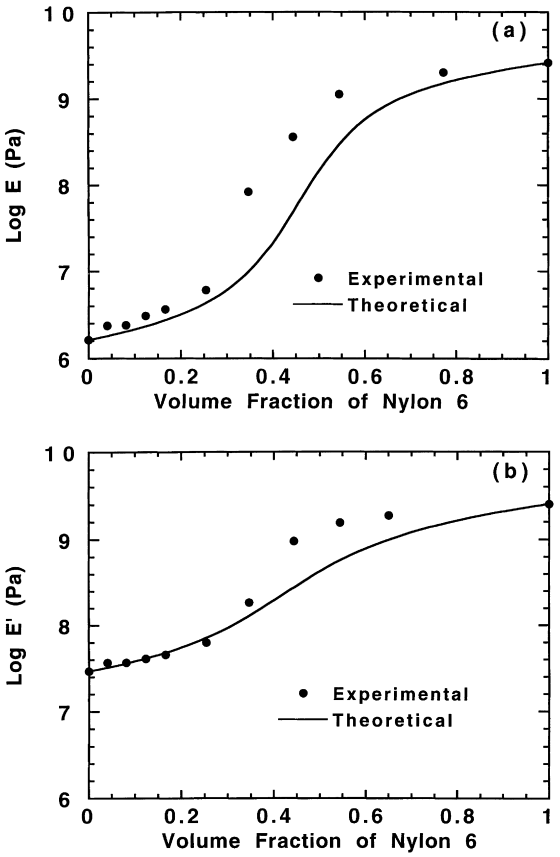

Fig. 18. Effect of nylon 6 content on: (a) Young's modulus, E, from stress–strain measurement and (b) dynamic storage modulus, E', for blends of $(100-x)$ vol% EPR-g-MA and x vol% nylon 6.

7. Conclusions

The morphology and physical properties of blends of nylon 6 and EPR-g-MA have been examined. As the content of nylon 6 is increased from 5 to 30%, the average size of the dispersed nylon 6 particles in the matrix of EPR-g-MA increased from 0.14 to 0.23 μm, while the hardness, modulus, and tensile strength of the blend increased. The observed values of the modulus are in reasonable agreement with those predicted by a theoretical model. As the content of nylon 6 increased from 30 to 50%, the physical properties of the blends change rapidly, due to phase inversion, i.e., the polyamide becomes the continuous phase with spherical, dispersed particles of EPR-g-MA.

The blends with an EPR-g-MA continuous phase have lower strength than commercial thermoplastic elastomers or TPE materials and show stress softening which indicates that the nylon 6 phase does not strongly reinforce the EPR-g-MA matrix. The blends based on a nylon 6 with reduced molecular weight made by a hydrolysis process showed somewhat improved strength and a reduced nylon particle size. The addition of magnesium oxide to these blends causes significant improvement in tensile properties. This may be the result of the reduced particle size caused by the

increase in melt viscosity or the formation of ionic cluster type crosslinks.

Acknowledgements

This research was supported by the US Army Research Office and Bridgestone Corp. The authors express their appreciation to AlliedSignal Inc., BASF Corp. and Exxon Chemical Co. for supplying various materials used in this research.

References

[1] Legge NR, Holden G, Schroeder HE, editors. Thermoplastic elastomers: a comprehensive review. New York: Hanser Publishers, 1987.
[2] Holden G, Legge NR. In: Legge NR, Holden G, Schroeder HE, editors. Thermoplastic elastomers: a comprehensive review. New York: Hanser Publishers, 1987:47–65.
[3] Morton M. Rubber Chem Technol 1983;56:1096.
[4] Cella RJ. J Polym Sci: Symp Ed 1973;42:727.
[5] Wells SC, editor. Handbook of thermoplastic elastomers. New York: Van Nostrand Reinhold, 1979:103–215.
[6] Wood AS. Modern Plastics 1985;62 (3):42.
[7] Bonart R. Angew Makromol Chem 1977;58/59:259.
[8] Bonk HW. In: Agranoff J, editor. Modern plastics encyclopedia 1984–85. New York: McGraw-Hill, 1985:100.
[9] Cooper SL, Huh DS, Morris WJ. Ind Eng Chem Prod Res Develop 1968;7:248.
[10] Puett D. J Polym Sci A-2 1967;5:839.
[11] Samuels SL, Wilkes GL. J Polym Sci: Symp 1973;43:149.
[12] Walker BM, editor. Handbook of thermoplastic elastomers. New York: Van Nostrand Reinhold, 1979.
[13] Wolkenbreit S. In: Walker BM, editor. Handbook of thermoplastic elastomers. New York: Van Nostrand Reinhold, 1979:216–46.
[14] Puett D, Smith KJJ, Ciferri A, Kontos EG. J Chem Phys 1964;40:253.
[15] Puett D, Smith KJ, Ciferri A. J Chem Phys 1965;69:141.
[16] Coran AY, Patel RP, Williams D. Rubber Chem Technol 1982;55:116.
[17] Rader CP. In: Harper CA, editor. Handbook of plastics, elastomers, and composites. New York: McGraw-Hill, 1996:51.
[18] Jha A, Bhowmick AK. Polymer 1997;38:4337.
[19] Lilaonitkul A, West JC, Cooper SL. J Macromol Sci Phys 1976;B12:563.
[20] Beecher JF, Marker L, Bradford RD, Aggarwal SL. Am Chem Soc, Polymer Preprints 1967;8:1532.
[21] Gaymans RJ. In: Collyer AA, editor. Rubber toughened engineering plastics. London: Chapman and Hall, 1994:210–42.
[22] Keskkula H, Paul DR. In: Collyer AA, editor. Rubber toughened engineering plastics. London: Chapman and Hall, 1994:136–64.
[23] Borggreve RJM, Gaymans RJ, Schuijer J, Housz JFI. Polymer 1987;28:1489.
[24] Oshinski AJ, Keskkula H, Paul DR. Polymer 1992;33:268.
[25] Oshinski AJ, Keskkula H, Paul DR. Polymer 1992;33:284.
[26] Oshinski AJ, Keskkula H, Paul DR. J Appl Polym Sci 1996;61:623.
[27] Oshinski AJ, Keskkula H, Paul DR. Polymer 1996;37:4891.
[28] Oshinski AJ, Keskkula H, Paul DR. Polymer 1996;37:4909.
[29] Oshinski AJ, Keskkula H, Paul DR. Polymer 1996;37:4919.
[30] Thamm RC, Buck WH. J Polym Sci, Polym Chem Ed 1978;16:539.
[31] Burlett DJ, Bauer RG, Kelley MM. US Patent 5,023,301, 1991 (assigned to the Goodyear Tire and Rubber Company).
[32] Burlett DJ, Pyle KJ, Sinsky MS, Bauer RG, Tung DA, Parameswaran VR. US Patent 5,268,134, 1993 (assigned to the Goodyear Tire and Rubber Company).
[33] Burlett DJ. Presentation at the Intersociety Polymer Conference, Baltimore, MD, 7–10 October 1995.
[34] Frazer WJ. Chem Ind 1966;33:1399.
[35] Haward RN, Mann J. Proc Phys Soc 1964;A282:120.
[36] Keskkula H. Appl Polym Symp 1970;15:51.
[37] Andrews EH, Fukahori Y. J Mater Sci 1977;12:1307.
[38] Beecher JF, Marker L, Bradford RD. J Polym Sci, Part C 1969;26:117.
[39] Kohan MI, editor. Nylon plastics handbook. New York: Hanser Publishers, 1995.
[40] Paterson MWA, White JR. J Mater Sci 1992;27:6229.
[41] Paterson MWA, White JR. Polym Eng Sci 1993;33:1475.
[42] Pezzin G. J Appl Polym Sci 1964;8:2195.
[43] Russel DP, Beaumont PWR. J Mater Sci 1980;15:208.
[44] Russel DP, Beaumont PWR. J Mater Sci 1980;15:197.
[45] Keskkula H. PhD Dissertation, University of Cincinnati, 1953.
[46] Coran AY, Endter CK. US Patent 4,661,554, 1987 (assigned to Monsanto).
[47] Morbitzer L, Ott KH, Schuster H, Kranz D. Angew Makromol Chem 1972;27:57.
[48] Morbitzer L, Kranz D, Humme G, Ott KH. J Appl Polym Sci 1976;20:2691.
[49] Beck RH, Gratch S, Newman S, Rusch KC. J Polym Sci, Polym Lett 1968;6:707.
[50] Wang TT, Sharpe LH. J Adhesion 1969;1:69.
[51] Kerner EH. Proc Phys Soc 1956;69B:808.
[52] Faucher JA. J Polym Sci: Polym Phys Ed 1974;12:2153.
[53] Hill R. J Mech Phys Solids 1965;13:213.
[54] Coran AY, Patel R. J Appl Polym Sci 1976;20:3005.
[55] Bucknall CB. Toughened plastics. London: Applied Science Publishers, 1977:118.
[56] Brandrup J, Immergut EH, editors. Polymer handbook, 3rd ed. New York: Wiley, 1989:V/113.
[57] Uemura S, Takayanagi M. J Appl Polym Sci 1966;10:113.